Reviewed Preprint
v1 • July 7, 2026
Not revised

For correspondence:
bwknowles@ucla.edu

* These authors contributed equally to this work.

Competing interests: No competing interests declared

Funding: See page 23

Reviewing editor: Curtis A Suttle, University of British Columbia, Canada

Central carbon metabolism switching in lytic versus temperate coral reef viral communities

Jacob Kelman[1,2,*], Meena Khan[1,2,*], Chibundu Umunna[1,2,*], Russell Brainard[3], Grace Donohue[1,2], Rob Edwards[4], Natalie A Falta[1,2], Emma George[5,6], Eleanor Gorham[1,2], Juris Grasis[7], Kevin Green[5], Andreas Haas[5,8], Kimberly Halsey[9], Eric Hester[5,10], Summer Jacob[1], Aydin Loid Karatas[1,2,11], Yan Wei Lim[5], Mark Little[5,12], Stuart Sandin[13], Jessie Segnitz[1], Maya Serota[1], Natalia Shahwan[1], Giselle Simmons[1], Jennifer E Smith[13], Isha Tripathi[1,2], Linda Wegley Kelly[13], Lauren Woodward[1], Nickie Yang[1,2], Charles Young[14], Brian Zgliczynski[13], Forest Rohwer[5], Ben Knowles[1,2,15,16]

[1]Department of Ecology and Evolutionary Biology, University of California, Los Angeles, Los Angeles, United States • [2]Institute for Quantitative and Computational Biosciences, University of California, Los Angeles, Los Angeles, United States • [3]R Ocean LLC, Kāne'ohe, United States • [4]Flinders Accelerator for Microbiome Exploration, Flinders University, Adelaide, Australia • [5]Biology Department, San Diego State University, San Diego, United States • [6]Integrative Oceanography Division, Scripps Institution of Oceanography, University of California, San Diego, San Diego, United States • [7]School of Natural Sciences, University of California, Merced, Merced, United States • [8]Department of Marine Microbiology and Biogeochemistry, NIOZ Royal Netherlands Institute for Sea Research, Den Burg, Netherlands • [9]Department of Microbiology, Oregon State University, Corvallis, United States • [10]NIZO Food Research B.V., Kernhemseweg, Netherlands • [11]Department of Quantitative and Computational Biology, University of Southern California, Los Angeles, United States • [12]Department of Organismic and Evolutionary Biology, Harvard University, Cambridge, United States • [13]Marine Biology Research Division, Scripps Institution of Oceanography, University of California, San Diego, San Diego, United States • [14]Pacific Islands Ocean Observing System, University of Hawaii at Manoa, Honolulu, United States • [15]California NanoSystems Institute, University of California, Los Angeles, Los Angeles, United States • [16]Institute of the Environment and Sustainability, University of California, Los Angeles, Los Angeles, United States

eLife Assessment

The worldwide decline in the health of coral reefs is well documented, and overgrowth by microbial consortia can be a contributing factor. Kelman and colleagues used metagenomic analysis to interrogate potential changes in phage-associated genes predicted to be involved in central carbon metabolism. The study addresses the hypothesis that metabolic genes associated with carbon metabolism that are encoded by viruses reflect the health of the corals. The study contributes a **valuable** perspective on the potential role of phages in coral health, although limitations of the data and analyses offer an exploratory examination rather than a definitive result. Overall, the evidence supporting the major findings is **incomplete**, in part because the conceptual model relies on qualitative assumptions rather than empirical data.

https://doi.org/10.7554/eLife.110377.1.sa2

Abstract

Coral reefs are declining globally due in part to bacterial overgrowth, a process known as microbialization. However, the role of bacteriophages that may inhibit microbialization by infecting and killing these bacteria remains poorly understood, especially their metabolic impacts on bacterial proliferation. To address this, we analyzed central carbon metabolism gene

frequencies in viral communities from healthy (lytic-dominated) and degraded (temperate-dominated) Central Pacific coral reefs. We found that viral metabolism shifted broadly from being dominated by metabolism that builds up pools of central intermediates on degraded reefs dominated by temperate viral infection ('anaplerotic' reactions) to metabolism that consumes these pools to prioritize production of metabolic precursors for virion construction on healthy reefs dominated by lytic infection ('cataplerotic' reactions). This switch was shown by the over-representation of Entner-Doudoroff (ED) glycolysis genes on degraded, temperate-dominated reefs and of pentose phosphate pathway (PPP) and reductive tricarboxylic acid cycle (TCA) genes on healthy, lytic-dominated reefs. As a result of this metabolic dichotomy, our qualitative compartment modeling revealed two distinct ecosystem states: (i) healthy reefs, where lytic viral metabolism enhances viral production and suppresses bacterial overgrowth, and (ii) degraded reefs, where temperate viral metabolism accelerates bacterial proliferation. Because viral switching between lytic and temperate lifestyles is a known function of host physiological state, these findings position viral metabolism as both a driver of reef decline and a conservation lever, with metabolically mediated 're-viralization' offering a novel strategy to restore reef resilience.

Significance

Coral reefs are collapsing worldwide, exacerbated by "microbialization," where algae-fueled bacteria overgrow corals. Viruses that infect these bacteria can suppress this process through lysis, but on degraded reefs they often switch to nonlethal temperate lifestyles, accelerating decline. Here we show that similar shifts occur in virus-encoded metabolism. On healthy reefs, lytic viruses carry genes that drain host metabolites to fuel virus production, which likely enhances infection and lysis rates and limits bacterial overgrowth. On degraded reefs, temperate viruses encode reactions that expand host metabolite pools, supporting bacterial proliferation. Thus, viral metabolism can either reinforce reef resilience or exacerbate collapse, making it a hidden driver of ecosystem fate and a potential target for conservation strategies.

Introduction

Ecosystem overgrowth by microbes, a process known as microbialization, is a major threat to coral reefs worldwide[1–2]. Microbialized reefs are subject to a positive feedback loop in which proliferating algae generate excess dissolved organic carbon (i.e., sugar) that fuels the growth of increasingly pathogenic and copiotrophic microbes that thrive in nutrient-rich environments[1,3,4]. This process exacerbates coral diseases and clears space for further algal growth[5–7].

Bacterial metabolism on degraded coral reefs is directed towards high-throughput rather than efficient carbohydrate utilization[1,8]. For instance, while bacterial metabolism on healthy reefs is dominated by genes for the efficient but multi-step Embden-Meyerhof-Parnas (EMP) pathway, degraded reefs exhibit greater representation of genes for the inefficient but short Entner-Doudoroff (ED) glycolysis pathway [1,9–11]. This shift on degraded reefs enable bacteria to readily exploit ecosystem organic carbon enrichment to build up cellular stockpiles of central metabolites like glyceraldehyde-3-phopshate (G3P) and pyruvate ('anaplerotic' reactions) as well as use those central metabolite pools to produce cellular energy such as ATP, reductants like NADH, and amino and nucleic acid biosynthetic precursors required for bacterial over-proliferation ('cataplerotic' reactions)[1,6,10].

Viral predation could, in principle, preclude microbialization by killing proliferating microbes, as lytic infection and lysis rates are predicted by established predator-prey models to rise with host densities and growth rates[12– 15]. However, viral communities switch from lytic to temperate infection during eutrophication and microbialization[13]. This transition towards non-lethal, temperate infection can facilitate further increases in microbial biomass due to suppressed lysis[13,16]. Further, temperate viral communities encode higher frequencies of pathogenicity genes that could protect bacteria from consumption by eukaryotic grazers[13,17–19]. These genes could facilitate microbialization by limiting protist predation, the major non-viral predation guild in the

ocean[20,21]. Altogether, rather than controlling bacterial populations, viruses may form a second 'Temperate Ratchet' feedback loop that traps ecosystems in persistent microbialization through suppressed lysis rates and protist grazing on pathogenic copiotrophs[13,22].

In addition to these population-level effects, viruses may also exert gene-level effects on microbialization by reshaping bacterial metabolism. Viruses shuttle a broad array of metabolic genes between hosts via horizontal gene transfer, thereby altering bacterial metabolism and ecology[23–26]. These include central carbon metabolism genes implicated in the metabolic switching of bacterial communities on microbialized reefs, such as the pentose phosphate pathway (PPP) and the ED and EMP glycolysis pathways[1,27]. In lytic viruses, these pathways support virion synthesis by converting general cellular metabolic pools like G3P and pyruvate to specialized metabolic precursors (i.e., they are cataplerotic reactions). For example, the PPP provides nucleic acid and amino acid precursors, whereas EMP generates cellular energy like ATP and NADH[26,28,29].

However, these genes can also be co-opted by bacteria during infection. As a result, while viral metabolic genes can combat microbialization by promoting the production of lytic viruses that would suppress bacterial abundance, they are also capable of exacerbating reef decline by enhancing bacterial proliferation. Together, these processes introduce a novel viral-mediated metabolic mechanism of reef decline or resilience beyond lytic-to-lysogenic switching.

However, the role of viral-encoded metabolic genes in coral reef microbialization remains unexplored. To address this gap, we leveraged 19 metagenomes of virus-like particles (VLPs; viromes) used in several prior publications[10,13,30], from Pacific coral reefs spanning a gradient from healthy to degraded states and from lytic to temperate infection dominance, to characterize changes in the frequencies of viral metabolic genes across a viral lifestyle spectrum. We found that temperate viral communities were enriched in anaplerotic central carbon metabolism genes, particularly those associated with copiotrophic growth like Entner-Doudoroff glycolysis and the generation of central metabolite pools that can be used for diverse cellular processes[31]. Lytic communities had higher levels of cataplerotic non-oxidative pentose phosphate pathway genes and oxidoreductases that generate specialized metabolic precursors, cellular energy and redox potential. Incorporating our findings into a conceptual model revealed that lytic viral metabolism can enhance viral production and microbial surveillance on healthy reefs ("viralization")[32], while temperate viral metabolism may accelerate microbialization in degraded systems. These findings implicate viral metabolism in feedback loops that either enhance reef resilience or exacerbate decline. Because viral lifestyle switching is a known function of cellular physiological state, with elevated nutrient availability driving non-lethal temperate infection, while nutrient limitation promotes lytic infection, our work suggests that metabolic management, such as limiting nutrient inputs, could promote rapid recovery of degraded reefs.

Methods

Metagenome sampling and processing

Metagenomes were sampled from virus-like particles (VLPs) from coral reefs across the central Pacific Ocean (n = 19; see Supplementary Table 1 for sample details) and samples processed as described previously[13,33]. For each viral metagenome, approximately 60-100 L of seawater were pumped from the reef surface into acid-washed, triple-rinsed low-density polyethylene bags and concentrated to < 500 mL using a 100 kDa tangential flow filter. Concentrates were then 0.45 µm-filtered to remove bacteria and 0.5 % final concentration chloroform was added to destroy any residual cells and extracellular vesicles[34]. Samples were stored at 4 °C until subsequent processing. The presence of concentrated VLPs was confirmed by epifluorescence microscopy of Sybr Gold stained viruses on anodisc filters[33].

VLPs were purified from concentrates using a cesium chloride step gradient approach[13,33,35]. The absence of cells in step gradient outputs was confirmed by microscopy. Purified samples were then DNAse I-treated at 37 °C for 2 hours and denatured at 65 °C for 15 minutes to remove extra-virion free DNA (peDNA; protected environmental DNA)[36]. Viral DNA was extracted using the

formamide/chloroform isoamyl alcohol technique[13,33,35]. The absence of contaminating host DNA in all samples was confirmed by the lack of PCR amplification of the universal 16S rDNA gene using primers 27F (AGA GTT TGA TCC TGG CTC AG) and 1492R (TAC GGY TAC CTT GTT ACG ACT T)[13,33,35]. Note that our analysis is based on correlations across many samples, minimizing the impact of any contamination on our findings. VLP DNA was amplified using the Linker Amplified Sequencing Library approach[18] prior to sequencing on an Illumina MiSeq platform.

Bioinformatic processing

Low-quality reads < 100 bp in length and with mean PHRED quality scores of < 25 were excluded using Prinseq[37]. Samples were then dereplicated with TagCleaner[38], human contaminants were removed using DeconSeq[39], and sequences were posted to MG-RAST (*www.mg-rast.org*; see Data Availability section). Accession numbers and summary statistics for the viral metagenomes used in this paper are shown in Supplementary Table 1.

Annotating metagenomes

Viral metagenomes were annotated by DIAMOND alignment against the SEED subsystems database on MG-RAST v4 using the default MG-RAST parameters as a very commonly used balance of accuracy and specificity[40]: e-value = −5 (annotated in MG-RAST as e-value = 5), 60 % identity, > 15 base length, a minimum abundance of 1, and all analyses conducted using representative hits (February 2020)[13,41]. Level 1 Gene categories with average frequencies below 0.5 % were omitted. Temperateness of each viral metagenome was assessed as the frequency of genes annotated in the Level 3 SEED category of "Phage_integration_and_excision" (i.e., how common genes involved in integration and excision were in each metagenome)[13]. The frequency of genes in high-order classification (e.g., SEED level 1 with categories shown in Figure 1) was calculated by summing the frequency of the genes making up each category. All analyses were normalized to account for different sequencing depth between samples. This was done by calculating gene frequency as the number of hits to a given gene divided by all known genes in that sample ("percent known")[14], making all analyses comparable and unaffected by the effects of varied sequencing depth between samples.

Pathway annotation

Pathway visualizations were guided by KEGG maps (*www.genome.jp/*), pathway-specific Wikipedia pages (*www.wikipedia.org/*), and enzyme Wikigenes entries (*www.wikigenes.org/*). Pathway maps were drawn using EC Number names of each enzyme (Table 1).

Anaplerotic and cataplerotic gene categorization

Genes were categorized based on whether they (i) generated central metabolite pools like glyeraldehyde-3-phopshate (G3P) and pyruvate ('anaplerotic' or 'filling up' reactions) that are flexibly used in multiple pathways by cells, or (ii) used these central metabolite pools to generate cellular energy or metabolic precursor products that are used for specific purposes (i.e., the products are 'used' metabolically; known together as 'cataplerotic' or 'drawing down' reactions), or (iii) were neither anaplerotic nor cataplerotic ('neither'). Note that although anaplerotic and cataplerotic reactions often refer to steps in the TCA, we are using the term more generally here[31].

Statistical analyses

The correlation between gene frequency, either at a Level 1 SEED category or individual gene level, and viral community temperateness were assessed using Spearman's Rho (ρ_s), a non-parametric rank-based measure of how monotonic the relationship between x- and y-values is (i.e., it is a non-parametric correlation coefficient). For supplementary diversity and photosynthesis gene analyses we estimated ρ_s using the R `cor.test()` function with exact = FALSE to avoid ties. For our main analyses shown in Table 1 and in Figures 1, 2, 3, and 4, we estimated ρ_s values using the `stat.spearmanr()` function in the Python `scipy.stats` package with bootstrapping to ensure robust median ρ_s assessment over 1000 iterations of

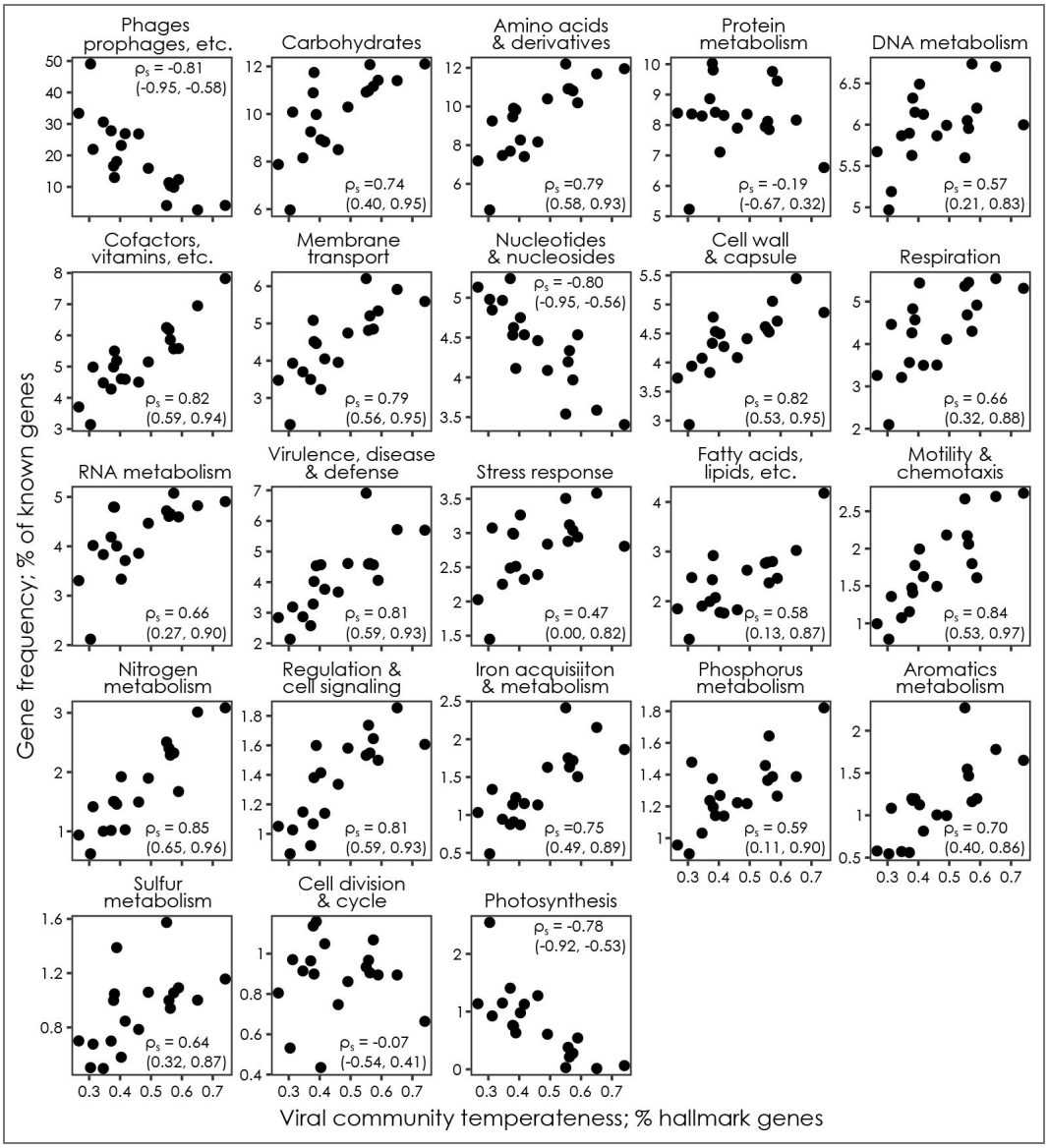

Figure 1. Correlations between metabolic function and community temperateness across the breadth of cellular metabolism.

Spearman's rho estimates (ρ_S) are shown with 95 % confidence intervals (CIs) in parentheses from 1,000 bootstrapped simulations. Panels are ordered by mean gene frequency. The y-axis shows the gene frequency as a percentage of known genes, an internally normalized and relative metric where all of the frequencies for a given sample across all panels sums to 100 %. Gene categories with average frequencies below 0.5 % were omitted. Viral community temperateness was calculated as the percentage of integrase and excision genes in the known genes in each virome. Genes where the 95 % confidence intervals exclude zero are significant at the $p < 0.05$ level. Bootstrapping code can be found at *https://github.com/hopefulmonstersucla/viral-metabolism/tree/main/code*.

EC number	SEED database gene name	Pathway	Gene activity	ρ_s	95 % CI	Observed in viruses
1.1.1.37	Malate dehydrogenase	Tricarboxylic Acid	Cataplerotic	-0.19	-0.61, 0.29	
1.1.1.41	Isocitrate dehydrogenase [NAD]	Tricarboxylic Acid	Cataplerotic	-0.13	-0.54, 0.34	
1.1.1.42	Isocitrate dehydrogenase [NADP]	Tricarboxylic Acid	Cataplerotic	-0.19	-0.63, 0.29	52,53
1.1.1.44	6-phosphogluconate dehydrogenase	Pentose Phosphate	Anaplerotic	-0.06	-0.54, 0.45	29,52,54
1.1.1.49	Glucose-6-phosphate 1-dehydrogenase	ED glycolysis/ Pentose Phosphate	Anaplerotic	0.26	-0.24, 0.68	
1.2.1.12	NAD-dependent glyceraldehyde-3-phosphate dehydrogenase	EMP glycolysis/ Gluconeogenesis	Cataplerotic	-0.20	-0.60, 0.26	
1.2.4.1	Pyruvate dehydrogenase	Tricarboxylic Acid	Cataplerotic	-0.12	-0.60, 0.36	52
1.2.4.2	2-oxoglutarate dehydrogenase	Tricarboxylic Acid	Cataplerotic	-0.10	-0.59, 0.42	
2.2.1.1	Transketolase	Pentose Phosphate		-0.08	-0.52, 0.35	29,52,54
2.2.1.2	Transaldolase	Pentose Phosphate	Cataplerotic	-0.49	-0.87, 0.02	7,45,47
2.3.3.1	Citrate synthase	Tricarboxylic Acid		0.15	-0.32, 0.56	
2.3.3.9	Malate synthase	Tricarboxylic Acid	Anaplerotic	0.61	0.20, 0.90*	55
2.7.1.11	6-phosphofructokinase	EMP glycolysis	Cataplerotic	-0.03	-0.48, 0.45	
2.7.1.40	Pyruvate kinase	EMP glycolysis	Cataplerotic	0.42	0.04, 0.74*	
2.7.2.3	Phosphoglycerate kinase	EMP glycolysis/ Gluconeogenesis	Cataplerotic	0.03	-0.41, 0.47	
3.1.1.31	6-phosphogluconolactonase	ED glycolysis/ Pentose Phosphate	Anaplerotic	0.43	0.03, 0.77*	
3.1.3.11	Fructose-1,6-bisphosphatase	Gluconeogenesis	Anaplerotic	0.24	-0.20, 0.66	55
4.1.1.31	Phosphoenolpyruvate carboxylase	Gluconeogenesis	Anaplerotic	0.45	0.00, 0.77*	
4.1.1.32	Phosphoenolpyruvate carboxykinase [GTP]	Gluconeogenesis		0.11	-0.39, 0.57	55,56
4.1.2.13 I	Fructose-bisphosphate aldolase class I	EMP glycolysis/ Gluconeogenesis	Cataplerotic	-0.65	-0.86, 0.33	
4.1.2.13 II	Fructose-bisphosphate aldolase class II	EMP glycolysis/ Gluconeogenesis	Cataplerotic	0.56	-0.18, 0.83	
4.1.2.14	2-dehydro-3-deoxyphosphogluconate aldolase	ED glycolysis	Anaplerotic	0.67	0.36, 0.90*	

Table 1. Central Carbon Metabolism genes shown in Figures 2 and 3.

Genes are categorized by pathway and gene function, identified by EC number and gene name, and annotated with prior references if they have been observed in viruses before. The Spearman's correlation between the frequency of each gene and viromes temperateness is indicated by bootstrapped mean ρ_s values and 95 % confidence intervals from 1,000 iterations are shown. Please refer to Supplementary Figure 2 for bootstrap ρ_s distributions. Genes where the 95 % confidence intervals exclude zero are significant at the $p < 0.05$ level. Genes shared between pathways are shown with a slash. Note, although anaplerotic and cataplerotic reactions often refer to steps in the TCA, we are using the term more generally here to refer respectively to the generation of central intermediate metabolites ('filling up'; anaplerotic) and the consumption of central metabolites to generate specialized pre-cursor or cellular energy pools ('drawing down'; cataplerotic) more generally[31]. Bootstrapping code can be found at *https://github.com/hopefulmonstersucla/viral-metabolism/tree/main/code*.

4.1.3.1	Isocitrate lyase	Tricarboxylic Acid		-0.10	-0.54, 0.37	
4.2.1.11	Enolase	EMP glycolysis/ Gluconeogenesis		0.43	0.02, 0.76*	[55]
4.2.1.12	Phosphogluconate dehydratase	ED glycolysis	Anaplerotic	0.71	0.47, 0.89*	
4.2.1.2	Fumarate hydratase class II	Tricarboxylic Acid		0.29	-0.15, 0.68	
4.2.1.3	Aconitate hydratase	Tricarboxylic Acid		-0.35	-0.71, 0.13	[55,57]
5.1.3.1	Ribulose-phosphate 3-epimerase	Pentose Phosphate		0.03	-0.45, 0.49	[58]
5.3.1.1	Triosephosphate isomerase	EMP glycolysis/ Gluconeogenesis		-0.02	-0.44, 0.41	[55]
5.3.1.6	Ribose 5-phosphate isomerase	Pentose Phosphate		0.32	-0.14, 0.68	[54]
5.3.1.9	Glucose-6-phosphate isomerase	EMP glycolysis/ Gluconeogenesis		0.45	0.12, 0.73*	
5.4.2.11	Phosphoglycerate mutase	EMP glycolysis/ Gluconeogenesis		-0.46	-0.80, 0.01	[55,56]
5.4.2.12	2,3-bisphosphoglycerate-independent phosphoglycerate mutase	EMP glycolysis/ Gluconeogenesis		0.41	-0.01, 0.73	
6.2.1.5a	Succinyl-CoA ligase [ADP-forming] alpha chain	Tricarboxylic Acid		0.17	-0.33, 0.61	
6.2.1.5b	Succinyl-CoA ligase [ADP-forming] beta chain	Tricarboxylic Acid		-0.04	-0.52, 0.41	

Table 1. (continued)

bootstrapping with replacement (see Supplementary Figure 2 for resulting distributions for central carbon metabolism genes). Confidence intervals of the median were assessed as the values corresponding to the 2.5th and 97.5th percentiles of the median values obtained from bootstrapping (95 % CI). For clarity, 95 % confidence intervals are listed in square brackets, as ρ_s [95 % CI minimum, 95 % CI maximum].

Bootstrapping code can be found at *https://github.com/hopefulmonstersucla/viral-metabolism/tree/main/code*. Note that correlations are significant at $p < 0.05$ when 95% bootstrap confidence intervals exclude zero, equivalent to classical null hypothesis testing.

Diversity metrics were assessed using the R vegan package, with the `diversity()` command used for Shannon diversity (natural log-transformed; H'). Median ρ_s at the pathway level were calculated as the median value of all of the ρ_s values for each enzyme in the pathway (i.e., they are a simple overall median).

Qualitative model

We created a conceptual model to demonstrate qualitative trends in bacterial, viral, coral, and algae abundance stemming from the changes in viral metabolism found here (Figure 5). Note that this model is not intended to be quantitative and was designed aid our understanding of trends in organismal abundance in response to the incorporation of viral metabolic capacity. Parameter values were implemented as high or low relative values to reflect known processes on healthy and degraded reefs (Supplementary Table 2 for parameter values). For example, high rates of disease[7,42] and bacterial metabolism[1] were used in degraded coral reef simulations, while high lysis rates were used in healthy systems[13,16].

Bacterial, viral, coral, and algae populations were initialized at 0.5 arbitrary units. The model was implemented using an iterative loop over six iterations (i.e., time in arbitrary units). This number of iterations was chosen as a balance of having enough iterations to see qualitative population trends, but without the need to make a more complicated model to generate long-term dynamics. At the beginning of each time step, new abundance values for each species (B_{new}, C_{new}, V_{new}) except algae were calculated based on the previous values (A_{new}). These updated values were applied at the end of each time step. Algae abundance was calculated last, occupying any remaining share of the benthos not occupied by coral. Once a population reached or fell below zero, it was excluded from further dynamics and not allowed to re-enter the ecosystem.

Code can be found at *https://github.com/hopefulmonstersucla/viral-metabolism/tree/main/code*.

For the 'no viruses' model shown in Figures 5a and 5d, we used the following equations, where terms with changed parameter values between Figures 5a and 5d are in bold (see Supplementary Table 2):

$$B_{\text{new}} = B + a^*A + m^*B \quad (1)$$

$$C_{\text{new}} = C + C^*C - i^*A - \mathbf{d}^*\mathbf{B} \quad (2)$$

$$A_{\text{new}} = 1 - C_{\text{new}} \quad (3)$$

In Equation 1, bacteria (B) proliferate due to carbon provided by algae, with carbon supply itself a product of algal population (A) as well as the rate of delivery (a). To make the model as conservative as possible, we did not vary the rate of carbon delivered to bacteria by the algae, although it likely is higher on degraded reefs and enhances bacterial grow more than shown by the model[9]. Bacterial proliferation is also enhanced by metabolic changes (m) reinforced by bacterial population size on degraded reefs[1]. Note that, in the absence of viruses the bacteria have no loss processes, including natural mortality, even though their proliferation may be constrained by a lack of algae to support growth.

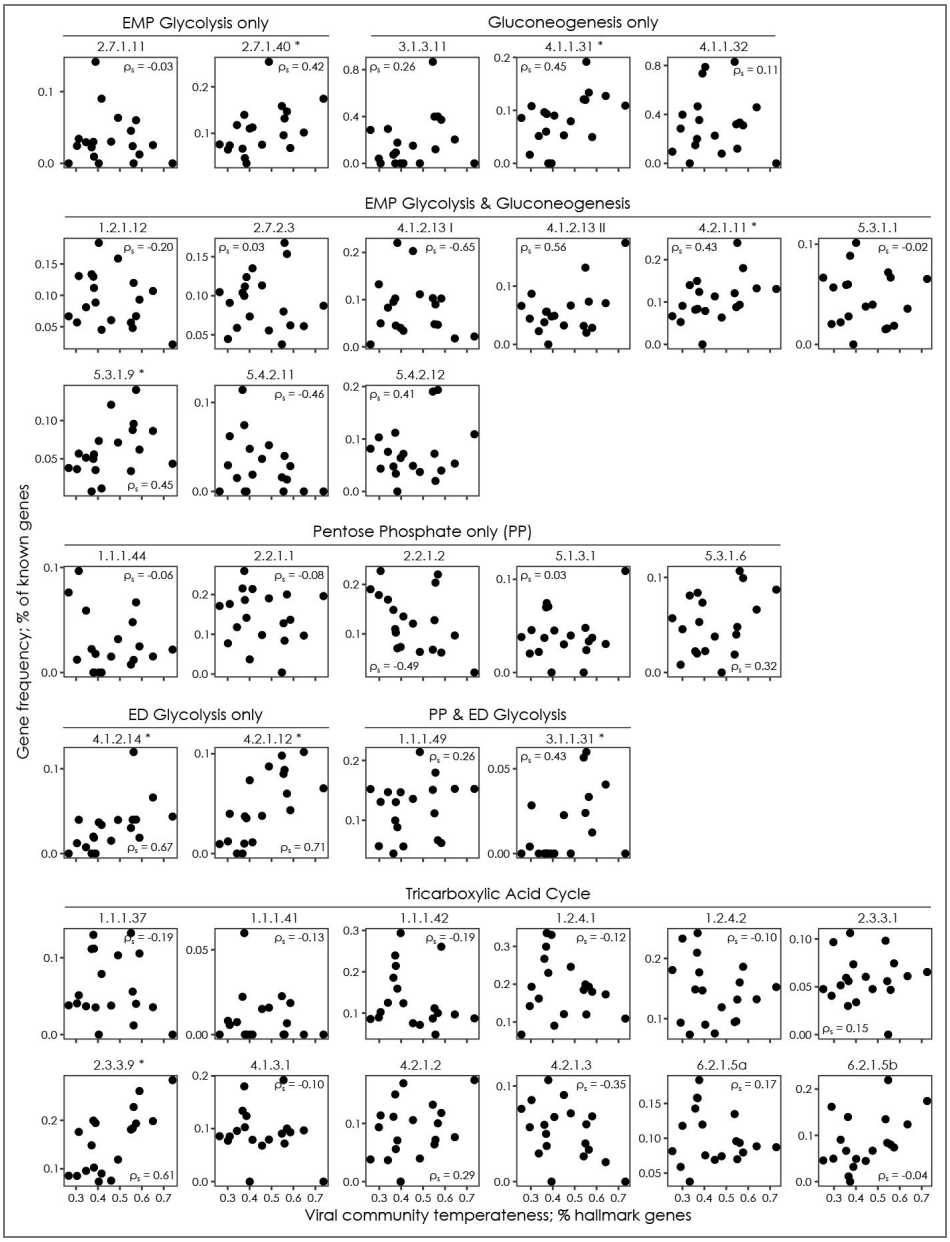

Figure 2. Correlation between central carbon metabolism genes and viral community temperateness.

Spearman's rho correlation coefficients (ρ_S) are shown from 1,000 bootstrapped simulations correlating central carbon metabolism gene frequency as a percentage of known genes vs viral community temperateness. Panels are ordered by pathway, including Embden-Meyerhof-Parnas glycolysis (EMP), Entner-Doudoroff glycolysis (ED), pentose phosphate (PP), and tricarboxylic acid cycle pathways. Viral community temperateness was calculated as the percentage of integrase and excision genes in the known genes in each virome. Enzymes with rho values significantly different to zero are indicated by asterisks (i.e., p< 0.05, 95 % confidence intervals exclude zero). Genes are labeled by EC numbers; see Table 1 for gene names and summary statistics.

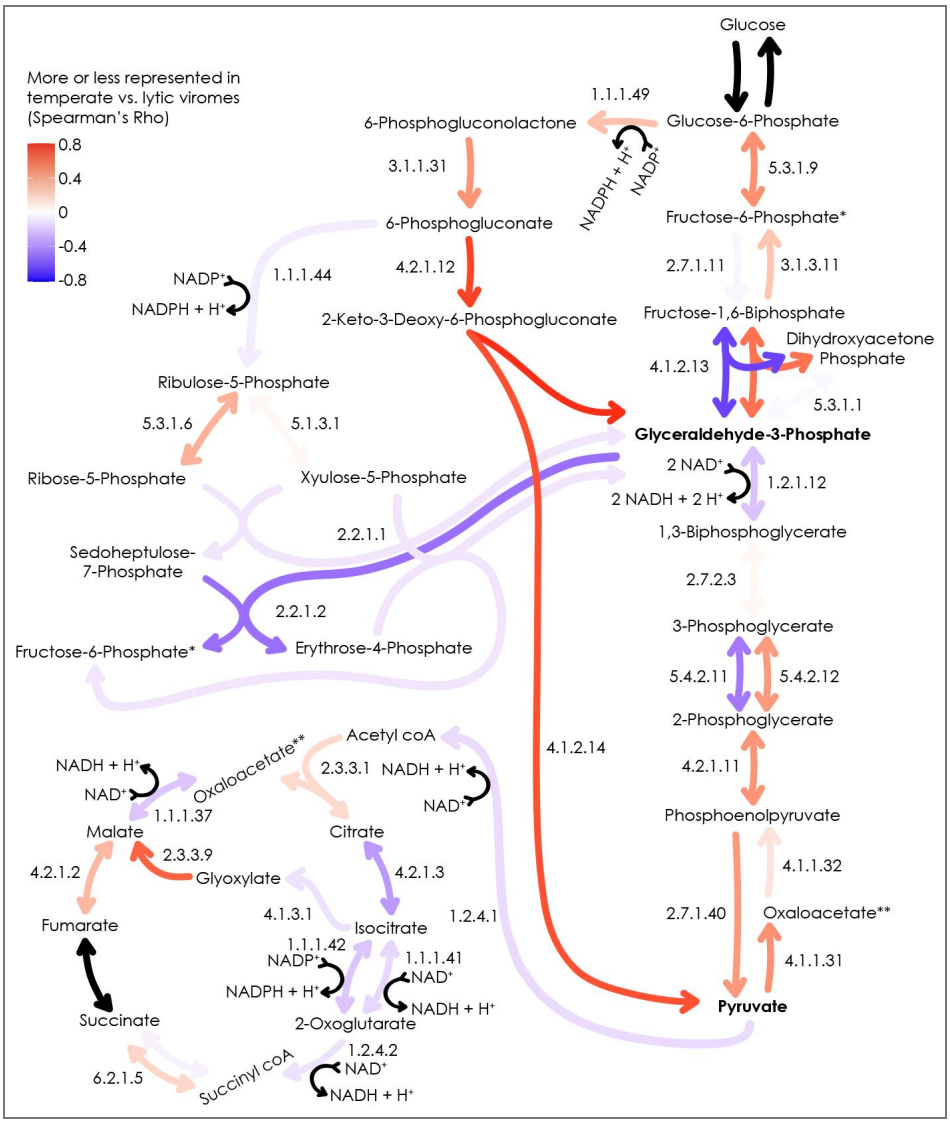

Figure 3. Pathway map of changes in the frequency of central carbon metabolism genes across the lytic to temperate spectrum.

Map of central carbon metabolism with each enzymatic step colored by the change in enzymatic metagenomic gene frequency across lytic to temperate viral communities. Red arrows show higher frequency in temperate communities while blue arrows are lytic associated, reflecting ρ_s values for each enzyme as seen in Table 1 and Figure 2. Enzymes are labeled by EC numbers (see Table 1 for gene names). Single-headed and double-headed arrows represent irreversible and reversible reactions, respectively. Black arrows show genes that were absent from all viromes. Central intermediate metabolites glyceraldehyde-3-phosphate (G3P) and pyryvate are shown in bold. *Note that fructose-6-phosphate is found in the EMP/gluconeogenesis pathways as well as the PPP, ** that oxaloacetate is produced in both the TCA and gluconeogenesis, and that EC1.1.1.42 in the TCA has an oxalosuccinate intermediate. Code can be found at *https://github.com/hopefulmonstersucla/viral-metabolism/tree/main/code*.

In Equation 2, coral populations (C) proliferate as a product of coral population size and growth rate (c). Coral growth is limited by algal population size and allelochemical inhibition (i)[43] as well as by bacterial pathogenicity causing coral disease (d)[7,44]. To make the model as conservative as possible, we did not alter the direct inhibitory effect of algae on coral across healthy and degraded reefs, although it is enhanced on unhealthy reefs[43,44].

In Equation 3, algal population size (A) is solved in the last step of each iteration as the remainder of the benthos not occupied by coral (1 – C) to account for the fact that the benthos is a finite space.

Note that Equations 2 and **3** are used for all iterations of the model with or without viral lysis and metabolism.

For the 'with lytic viruses' model shown in Figures 5b and 5e we used the following equations, with bold terms reflecting varied parameter values and with new terms compared to Equations 1 and Equation 2 underlined:

$$B_{\text{new}} = B + a^{*}A + \mathbf{m}^{*}\mathbf{B} \underline{- \mathbf{k}^{*}\mathbf{V}} \tag{4}$$

$$\underline{V_{\text{new}} = V + k^{*}\mathbf{B}} \tag{5}$$

Building on Equation 1, lytic viruses are introduced in Equation 4 as a mortality term for bacteria as an outcome of viral population size (V) and lysis rate (k).

A viral population (V) is added to the model in Equation 5, where viruses proliferate at burst size (k) from lysis if bacteria. Note that k changes between healthy and degraded reef scenarios, consistent with Piggyback-the-Winner dynamics suppressing lysis on degraded reefs[13].

For the 'with viral lysis and metabolism' model shown in Figures 5c and 5f we used the following equations, with bold terms reflecting varied parameter values and with new terms compared to Equations 4 and 5 underlined:

$$B_{\text{new}} = B + a^{*}A + \mathbf{m}^{*}\mathbf{B} - \mathbf{k}^{*}\mathbf{V} \underline{+ \boldsymbol{t}^{*}\mathbf{V}} \tag{6}$$

$$V_{\text{new}} = V + k^{*}\mathbf{B} \underline{+ I^{*}\mathbf{V}} \tag{7}$$

This model builds on Equation 4 by adding viral metabolic function (t) that enhances bacterial proliferation in degraded reef scenarios associated with temperate Piggyback-the-Winner dynamics in Equation 6[13]. Equation 7 builds on Equation 5 by adding lytic functions that enhance virion production in healthy reefs (l).

Results

Hallmarks of viral temperateness

To assess how viral metabolism across the lytic-temperate spectrum could affect coral reefs, we examined how the fraction of sequenced reads that mapped to known genes in broad metabolic categories (SEED Database Level 1 annotation) changed with community temperateness. Building on prior work[13], we used the frequency of integrase and excisionase genes as a proxy for community temperateness (i.e., hallmarks of temperateness) in viral communities across the Central Pacific Ocean (Supplementary Table 1). As a measure of how consistently or monotonously gene frequency and sample temperateness covary, Spearman Rho (ρ_s) values reflect the strength and sign of their correlation. In this analysis, temperate-associated genes have positive correlations ($\rho_s > 0$) while lytic-associated genes have negative correlations ($\rho_s < 0$. For

clarity, 95 % confidence intervals are listed in square brackets as ρ_s [95 % CI minimum, 95 % CI maximum], and correlations where the confidence intervals exclude zero are significant at the $p < 0.05$ level.

Gene names and corresponding pathways, EC numbers, median ρ_s and 95 % CIs, gene category (anaplerotic vs cataplerotic), and reports of the gene in viruses are shown in Table 1. Figure 1 and Figure 2 display the sample-level patterns of temperateness vs gene frequency in all Level 1 SEED categories and in central carbon metabolism functions, respectively. The correlations shown in Figure 2 are represented in a metabolic pathway map in Figure 3 and analyzed according to Table 1 categories in Figure 4. Finally, the implications of our central findings are incorporated into a schematic ecosystem model shown in Figure 5.

Temperate viral communities are enriched in metabolic genes

The frequency of genes in the Phages, Prophages, Transposable Elements, and Plasmids category declined with increasing temperateness of viral communities (Figure 1; $\rho_s = -0.81$ [−0.95, −0.58]). In contrast, the frequency and diversity of 'bacterial' metabolic genes that encode known cellular functions increased in temperate viral communities (Supplementary Figure 1; $\rho_s = 0.63$ and 0.81, respectively; c.f., genetic diversity declines with temperateness when unknown genes are included[13]). Altogether, this analysis indicates that temperate viral communities are more metabolically similar to bacteria than are lytic communities.

Functional homologues as viral lifestyle markers

Analogous to taxonomic markers in cells, where the prevalence of class I and class II homologues of fructose bisphosphate aldolase EC4.1.2.13 genes relates to bacterial taxonomy[45], the divergent correlations in these genes across a viral temperateness spectrum may reflect viral life strategies (EC 4.1.2.13 I $\rho_s = -0.65$ [−0.86, 0.33] while EC4.1.2.13 II $\rho_s = 0.56$ [−0.18, 0.83]; see Table 1 for summary statistics).

Photosynthesis genes in lytic communities

The decline in 'Phages, Prophages, Transposable Elements, and Plasmid' genes from ~ 50 % of the known genes in lytic viromes to ~ 5 % in temperate viromes caused the gene frequency in almost all other categories to increase (as total gene frequencies sum to 100 %; 17 of 22 categories had $\rho_s > 0.5$; Figure 1). A notable exception is Photosynthesis genes: these had higher frequencies in lytic communities vs. temperate communities in the Level 1 analysis ($\rho_s = -0.78$ [−0.92, −0.53]; Figure 1). Photosynthesis genes, including rhodopsins, were also lytic-associated at the individual-gene level, where 16 out of 20 photosynthesis genes had negative ρ_s values (Supplementary Table 3). Finally, photosynthesis-related electron transport (Pet) genes that couple Photosystems II and I are absent from the viromes (Supplementary Table 3).

Carbohydrate metabolism genes

Given the high prevalence of carbohydrate genes in the viromes, their elevated frequency in temperate communities (Figure 1; $\rho_s > 0$), and their ecological importance, we next focused on genes comprising central carbon metabolism[25,26] Embden-Meyerhof-Parnas (EMP) and Entner-Doudoroff (ED) glycolysis pathways, the pentose phosphate pathway (PPP) and the Tricarboxylic Acid Cycle (TCA; Figure 2). Note that for this and subsequent analyses we retained only sequences with hits to SEED database entries with high-confidence Enzyme Commission (EC) annotations[46].

Entner-Doudoroff genes are enriched in temperate viromes

Few patterns were readily apparent from the ρ_s values for genes in each pathway (Figure 2; Supplementary Figure 2). When viewed as a pathway map, though, the ED pathway was more clearly enriched in temperate viral communities (i.e., the red arrows running through the center of Figure 3). This map identified the ED pathway as the only pathway that changed consistently across the lytic-temperate spectrum (Figure 4a), and was exclusively over-represented in

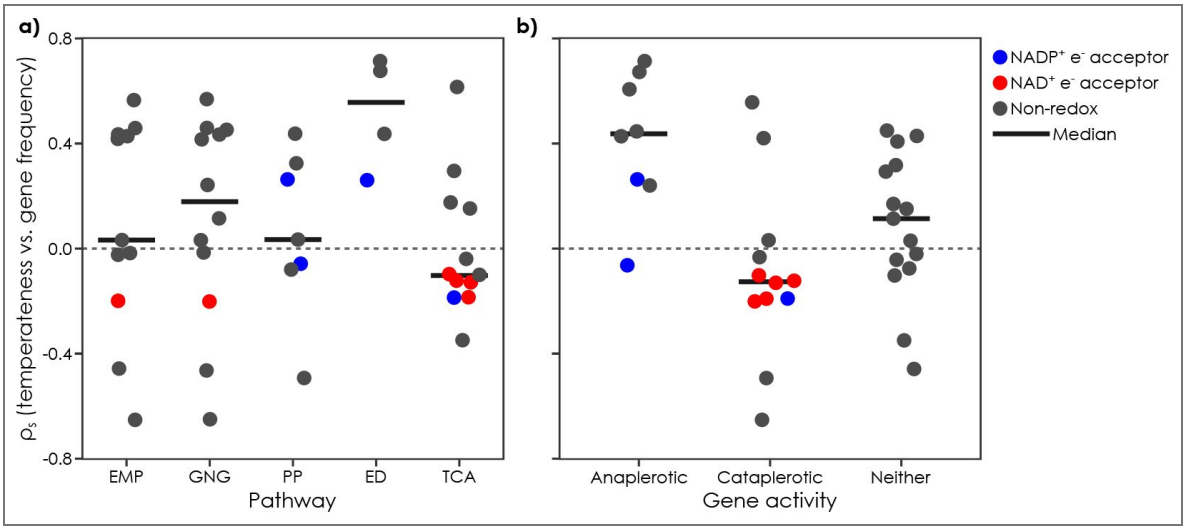

Figure 4. Correlations between viral community temperateness and central carbon gene frequency across pathways and gene function.

(a) Spearman's rho correlation coefficients (ρ_s) for genes in the Embden-Meyerhof-Parnas glycolysis (EMP), gluconeogenesis (GNG), pentose phosphate (PP), Entner-Doudoroff glycolysis (ED, and tricarboxylic acid cycle (TCA) pathways are shown with median values marked by horizontal bars in each pathway. (b) Coefficients are also shown for genes involved in building up central intermediate metabolite pools like pyruvate and glyceraldehyde-3-phosphate (anaplerotic reactions) or consuming general metabolites to make specialized pools of precursors and cellular energy (cataplerotic reactions) in central carbon metabolism, compared with genes involved in neither anaplerosis nor cataplerosis, also with median values shown. Oxidoreductase genes are colored by their electron acceptor: blue for $NADP^+$ electron acceptors involved in biomass generation, and red for NAD^+ electron acceptors involved in cellular energy generation. Dashed horizontal lines indicate ρ_s = 0. Note, although anaplerotic and cataplerotic reactions often refer to steps in the TCA, we are using the term more generally here to refer respectively to the generation ('filling up'; anaplerotic) of flexible general intermediate metabolites and the consumption of general metabolites towards precursor and cellular energy production ('drawing down'; cataplerotic) more generally[31].

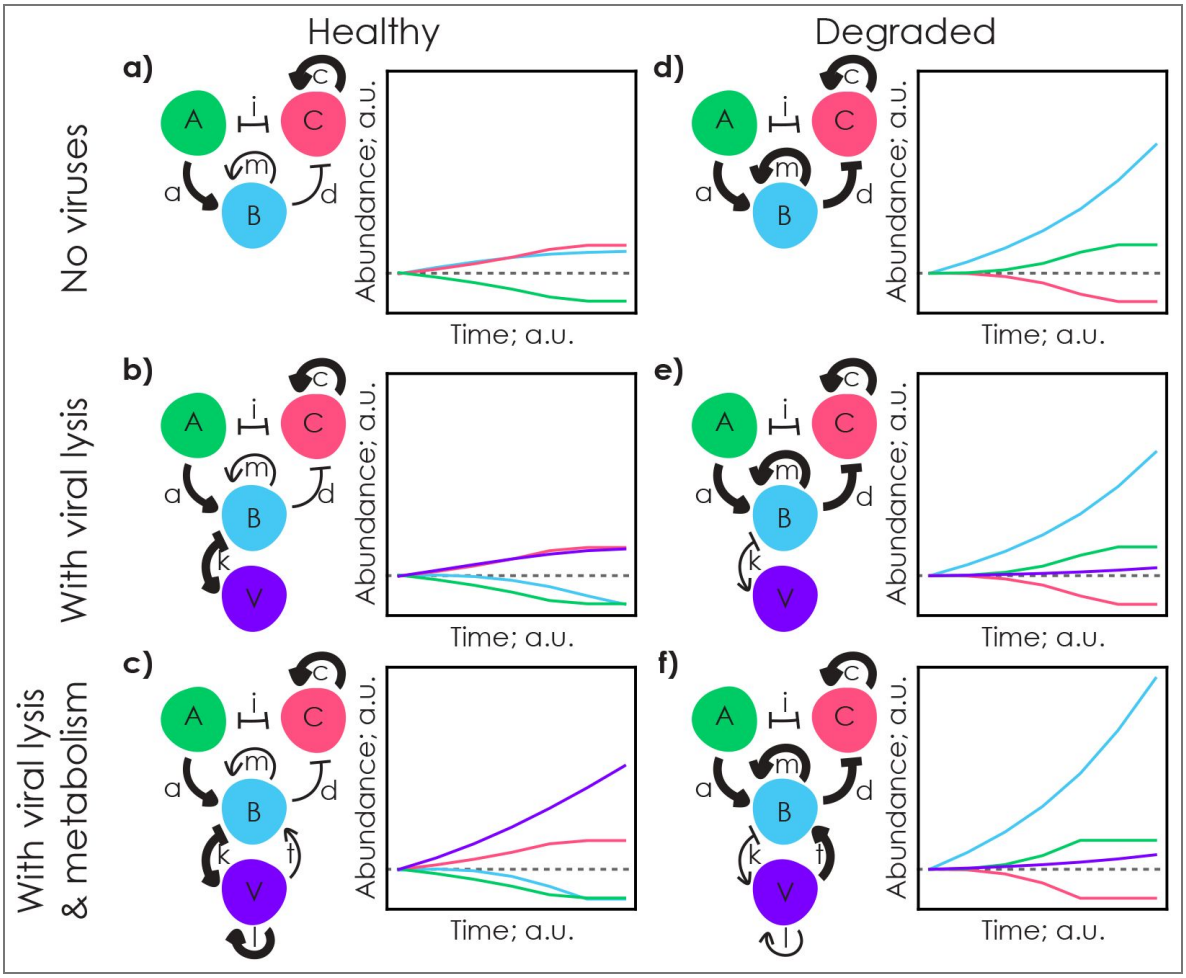

Figure 5. Schematic model incorporating viral metabolic effects on resilience of healthy coral reefs and exacerbation of reef degradation.

The predicted effects of viral lysis and metabolic capability on algal (A; green), coral (C; coral), bacteria (B; blue) and viral (V; violet) population sizes in healthy and degraded reef scenarios with no viruses (a and d, respectively), with viral lysis (b and e, respectively), and with viral lysis and metabolism (c and f, respectively). Compartment models showing how the model was implemented for each panel are shown (left) as well as resulting dynamics (right). Dynamics show changes in populations over time, in arbitrary units (a.u.), reflecting the qualitative nature of the model. In each iteration, algal population size A was solved as the 1 – C to reflect the finite space available on the benthos. Parameter values, shown as line weights, qualitatively reflect known processes on healthy vs degraded reefs, and can be found in Supplementary Table 2. Rates include: (i) coral-algal inhibition, (c) coral proliferation, (a) algal-mediated DOC supply to bacteria, (m) bacterial anabolic metabolism, (d) bacterial-mediate coral disease, (k) viral lysis of bacteria, (l) lytic viral metabolism, and (t) temperate viral metabolism. Note that panels **(b)** and **(e)** depict the Kill-the-Winner and Piggyback-the-Winner models, respectively. Algal, coral, bacteria, and viral pools were initialized at 0.5 a.u. for all simulations where present. To make the model as conservative as possible, rates of algal carbon delivery (a), and direct coral-algal interference (i) were not changed across scenarios; doing so would lead to enhanced loss of coral. Note that flat lines at minimal values reflect functional population extinction.

temperate viral communities (i.e., $\rho_s > 0$; EC 1.1.1.49 $\rho_s = 0.26$ [−0.24, 0.68], EC3.1.1.31 $\rho_s = 0.43$ [0.03, 0.77], EC4.1.2.14 $\rho_s = 0.67$ [0.36, 0.90], and EC4.2.1.12 $\rho_s = 0.71$ [0.47, 0.89]). Altogether, this gave the ED pathway an overall median $\rho_s = 0.55$ in contrast to overall median $\rho_s = 0.03$ for EMP glycolysis, $\rho_s = 0.175$ for gluconeogenesis (GNG), $\rho_s = 0.03$ for the PPP, and $\rho_s = -0.10$ for the TCA (see Figure 4a).

Anaplerotic temperate metabolism

Given the role of ED glycolysis in generating central metabolite pools for use in diverse pathways (i.e., ED is an anaplerotic pathway), we investigated whether temperate viral communities were enriched in anaplerotic genes more generally (see Table 1 for a list of anaplerotic and cataplerotic genes)[31]. Temperate viral communities were, indeed, enriched in anaplerotic genes, with an overall median $\rho_s = 0.44$ for anaplerotic reactions and only one gene even weakly lytic associated (6-phosphogluconate dehydrogenase EC 1.1.1.44 from the PPP; $\rho_s = -0.06$ [−0.54, 0.45]; Figure 4b).

Amino acid precursor genes are enriched in lytic viromes

In contrast to the ED-enrichment of temperate communities, the pathway map does not show many areas of contiguous lytic-associated genes (Figure 3). However, the enrichment of non-oxidative PPP genes in lytic communities, especially transaldolase EC 2.2.1.2 ($\rho_s = -0.49$ [−0.87, 0.02]). This enzyme consumes the central metabolite pool of glutaraldehyde-3-phosphate (G3P) to produce fructose 6-phosphate and erythrose 4-phosphate. Given that other fructose-6-phosphate producing genes are not similarly enriched in lytic communities (e.g., EC 2.2.1.1 in the PPP ρ_s = −0.08 [−0.52, 0.35], EC5.3.1.9 in EMP $\rho_s = 0.45$ [0.12, 0.73], and EC3.1.3.11 in gluconeogenesis ρ_s = 0.24 [−0.20, 0.66]), this suggests that the primary outcome of the non-oxidative PPP in lytic viral communities is the cataplerotic consumption of G3P for the generation of erythrose-4-phosphate, a precursor for amino acid biosynthesis[47].

Redox genes are over-represented in lytic communities

Given this cataplerotic focus in lytic communities, we investigated whether lytic communities were more strongly associated with individual cataplerotic reactions regardless of pathway rather than with whole pathways. Focusing on the distribution of anabolic redox steps across all the central carbon metabolism pathways, we found that NADPH-generating reactions were not consistently associated with either lytic or temperate communities (EC1.1.1.44 $\rho_s = -0.06$, EC1.1.1.42 $\rho_s = -0.19$, and EC1.1.1.49 $\rho_s = 0.26$, giving a median $\rho_s = -0.06$). In contrast, NADH-producing oxidoreductase genes were universally over-represented in lytic communities (i.e., all $\rho_s < 0$; median $\rho_s = -0.13$ across all NADH-producing reactions from EC1.1.1.37 $\rho_s = -0.19$ [−0.61, 0.29], EC1.1.1.41 $\rho_s = -0.13$ [−0.54, 0.34], EC1.2.1.12 $\rho_s = -0.20$ [−0.60, 0.26], EC1.2.4.1 $\rho_s = -0.12$ [−0.60, 0.36], EC1.2.4.2 $\rho_s = -0.10$ [−0.59, 0.42]; Table 1; Figures 2, 3, and 4). This included all redox genes in the TCA being lytic associated (i.e., $\rho_s < 0$, with an overall median $\rho_s = -0.13$) in contrast to the other, non-oxidoreductase genes which had a median $\rho_s = 0.15$, highlighting the specific overrepresentation of redox genes in lytic communities (Figure 4a).

Cataplerotic lytic metabolism

Given the association between lytic communities and cataplerotic reactions observed in the PPP and the TCA, we then investigated whether lytic communities are broadly enriched in cataplerotic genes. We observed that the overall median ρ_s of cataplerotic reactions was −0.125 (i.e., these genes were enriched in lytic communities) compared to $\rho_s = 0.44$ and $\rho_s = 0.11$ for anaplerotic reactions and reactions that are neither cataplerotic nor anaplerotic, respectively. This result highlights the association between lytic viral communities and cataplerotic metabolism.

Implications for Healthy Coral Reefs

To qualitatively describe the ecosystem effects of viral metabolism, we constructed a schematic model of algal-bacterial-viral-coral interactions, with all population sizes measured in illustrative arbitrary units (Figure 5). Parameterizing the model to healthy reef values (Figure 5a; note that parameterization of the healthy reef scenario largely insulates coral from the effects of bacterial overgrowth due to the small d value used; see Supplementary Table 2 for parameters and values)[1,7,8,13,42], the system became coral-dominated by t = 5, with coral-bacterial coexistence (coral and bacteria had increased from 0.5 a.u. initial values to 1.0 a.u. and 0.89 a.u., respectively, by t = 6). While the addition of viral lysis (Figure 5b) did not markedly change coral or algal dynamics, it led to the extinction of bacteria by t = 6 and to an ecosystem dominated by coral and viruses (coral and viruses had increased from 0.5 a.u. to 1.0 a.u. and 0.97 a.u., respectively, by the end of the simulation). Finally, adding in viral metabolism led to an earlier extinction of bacteria (by t = 5) and enhanced viral population size (viruses were 2.29 a.u. by t = 6), although coral and algal population dynamics were unaffected (Figure 5c). Altogether, the model recaptured the coral-dominated status of healthy coral reefs and showed that viral metabolism likely exerts a profound negative effect on bacterial populations and a strongly positive effect on viral populations on healthy reefs.

Implications for Degraded Coral Reefs

In contrast to healthy systems, our model suggests that degraded coral reefs would be overgrown with algae rather than coral (Figure 5). Note that the parameterization of the degraded reef scenarios leads to enhanced deleterious bacterial effects on coral health. Coral went extinct by t = 5 in the degraded scenarios without viruses and with viral lysis only (Figure 5d and e), as algal overgrew the benthos and bacterial proliferated to levels much higher than in any of the healthy scenarios (B = 2.75 a.u. and 2.64 a.u. in the no virus and lysis-only models, respectively, by t = 6). In contrast to bacteria, viral populations did not proliferate markedly in the viral-lysis model, increasing from 0.5 a.u. to only 0.64 a.u. by t = 6 (Figure 5e). Adding in viral metabolism that enhanced bacterial proliferation (t) allowed bacteria to proliferate even further (reaching 3.80 a.u.), supporting a modest rise in viruses (to 0.75 a.u.), and driving the coral to extinction sooner (by t = 4; Figure 5f). Altogether, our qualitative model suggests that viral metabolism supporting bacterial proliferation can enhance microbial overgrowth of reefs and promote shifts towards algal dominance of the benthos.

Discussion

The role of microbial overgrowth in coral reef decline is well established[1–2,7]. It is further intensified by shifts in bacterial metabolism and viral lifestyles that promote bacterial proliferation[13,16]. Here, we show that this process is further exacerbated by viral-encoded metabolic genes, whereas healthy ecosystems may be protected by viral lysis and metabolic genes that enhance virion production. Because temperate viral infection is tightly linked to host physiology and environmental conditions such as nutrient availability[13,48,49], targeting bacterial metabolic states through manipulation of nutrients could enable a shift in viral effects from degradative to protective, presenting a promising new conservation strategy.

Viruses become increasingly temperate on degraded reefs, following Piggyback-the-Winner (PtW) dynamics[13,22], in which abundant, rapidly proliferating bacterial hosts select for non-lethal, lysogenic infection. This switch in viral lifestyle suspends the top-down control exerted by lytic viruses, allowing bacterial populations to expand unchecked by lethal infection[13,49]. Temperate infection not reduces lysis but also promotes horizontal gene transfer of pathogenicity genes[50], which can help bacteria evade predation by eukaryotic grazers and potentially compromise coral health[13,22]. This forms a positive feedback loop wherein bacterial growth triggers viral lifestyle switching, which in turn facilitates further bacterial growth, establishing a 'Temperate Ratchet'[22] that locks ecosystems into ever-exacerbating bacterial overgrowth and coral disease[13]. Worse,

here we show that the temperate viruses on degraded reefs also harbor metabolic genes, such as those for Entner-Doudoroff glycolysis, that can directly support bacterial proliferation and overgrowth of reefs[1], thereby enhancing the Temperate Ratchet[22].

Healthy reefs, in contrast, appear to be guarded by lytic viruses. Lytic infection rates are driven by virus-host predator-prey encounter frequencies that are the outcome of host and viral abundances[12–14]. As a result, as bacterial populations grow, so should lytic infections and lysis, precluding bacterial overgrowth[13,16]. Further, the viral communities on healthy reefs do not harbor the high frequency of pathogenicity genes seen on degraded reefs, meaning that grazing and coral health are not being hindered by viral-encoded genes, which also helps to keep bacterial densities low[7]. Here we show that lytic viral communities on healthy reefs are enriched in metabolic genes associated with efficient energy production and biosynthesis, such as those for the Embden-Meyerhof-Parnas glycolysis pathway[1,9] and oxidoreductases involved in ATP generation and NADH reduction[51]. These metabolic features support robust virion production that can support reef 'viralization' through high viral abundances and high rates of virus-host encounters, infection, and lysis. In this way, lytic viral metabolism and reef viralization acts as a counterbalance to the Temperate Ratchet, helping to stabilize healthy reef ecosystems[32].

Viral metabolism associated with the lytic-to-temperate shift likely exacerbates coral reef decline, as shown here. Building on ecosystem-scale processes like viral lifestyle switching[13,16], the metabolic capacity of temperate and lytic viruses can further drive reefs into two stable states: healthy reefs protected by metabolically enhanced lytic control of bacteria, and degraded reefs ratcheted into persistent microbialization under temperate infection and metabolism. Ultimately, degraded coral reefs experience a metabolic disorder, where excess nutrients trigger ecosystem-scale dysregulation through microbial and viral lifestyle and metabolic switching[1–2,6]. However, the physiological basis of this switch also suggests that conservation measures targeting nutrient supply could undercut copiotrophic bacterial and viral metabolism[3,9,10]. Our findings suggest that doing so could lead to a 're-viralization' of the reef system, harnessing viral metabolic and lifestyle switching to enhance reef restoration and resilience.

Data Availability

Viral metagenomes can be found on MG-RAST under the accession numbers 4683670.3, 4683674.3, 4683677.3, 4683680.3, 4683683.3, 4683684.3, 4683686.3, 4683703.3, 4683704.3, 4683712.3, 4683718.3, 4683720.3, 4683731.3, 4683733.3, 4683745.3, 4683746.3, and 4683747.3 (see Supplementary Table 1 for library data summaries; *www.mg-rast.org*). Fasta files for each sample, statistical and modeling code, and annotations and simulations data can be found at *https://github.com/hopefulmonstersucla/viral-metabolism*.

Supplementary Tables and Figures

Sample Location	MG-RAST Accession Number	bp count	Sequence count	Latitude	Longitude
Millennium Atoll	4683670.3	47624434	173813	-9.9138	-150.2038
Flint Atoll	4683674.3	7294624	26673	-11.43	-151.8192
Starbuck	4683677.3	28130343	102666	-5.6384	-155.8811
Maui	4683680.3	48918703	178536	20.86447	-156.13911
Oahu	4683683.3	28708747	104972	21.4389	-158
Pearl & Hermes Reef	4683684.3	211441921	771690	27.8557	-175.8318
Kaui	4683686.3	14722075	53831	22.0964	-159.5261
Starbuck	4683703.3	51673568	188592	-5.6384	-155.8811
Niihau	4683704.3	17098607	62505	21.85115	-160.18327
Molokai	4683712.3	31626104	115424	21.17481	-156.8214
Lisianski	4683718.3	51289619	187189	25.98702	-173.99438
Malden Atoll	4683720.3	68368950	249522	-4.0123	-154.9178
French Frigate Shoals	4683731.3	12353528	45131	23.87748	-166.29115
Hawaii	4683733.3	30728163	112147	20.00324	-155.83318
French Frigate Shoals	4683745.3	64763334	236363	23.6417	-155.8778
Lanaii	4683746.3	38160746	139273	20.76167	-156.8334
Millenium Atoll	4683747.3	71166319	259736	-9.9138	-150.2038
Pearl & Hermes Reef Wreck*	4574481.3	24339533	88980	27.8666	-175.7468
Caroline Wreck Site*	4574475.3	11555298	42262	-9.9957	-150.2161

Supplementary Table 1. Summary of the 19 samples analyzed, including sample accession numbers, the total number of base pairs, reads sequenced, and locations of viral metagenomes. Note that all metagenomes have been previously published except Pearl and Hermes Reef Wreck and Caroline Wreck Site samples indicated by an asterisk. Caroline Island is now named Millenium Atoll. Fasta files for all metagenomes can be found at *https://github.com/hopefulmonstersucla/viral-metabolism/tree/main/fastas*.

Parameter	Symbol	Healthy reef without viruses	Degraded reef without viruses	Healthy reef with viruses	Degraded reef with viruses	Healthy reef with viruses and viral metabolism	Degraded reef with viruses and viral metabolism
Bacterial replication	m	0.02	0.2	0.02	0.2	0.02	0.2
Bacterial inhibition of coral	d	0.02	0.2	0.02	0.2	0.02	0.2
Coral replication	c	0.2	0.2	0.2	0.2	0.2	0.2
Algal inhibition of coral	i	0.02	0.02	0.02	0.02	0.02	0.02
Algal support of bacteria	a	0.2	0.2	0.2	0.2	0.2	0.2
Viral replication	l	-	-	-	-	0.2	0.02
Viral lysis of bacteria	k	-	-	0.2	0.02	0.2	0.02
Bacterial support of viral replication	k	-	-	0.2	0.02	0.2	0.02
Viral support of bacterial replication	t	-	-	-	-	0.02	0.2
Bacterial initial population	B	0.5	0.5	0.5	0.5	0.5	0.5
Coral initial population	C	0.5	0.5	0.5	0.5	0.5	0.5
Algal initial population	A	0.5	0.5	0.5	0.5	0.5	0.5
Viral initial population	V	-	-	0.5	0.5	0.5	0.5

Supplementary Table 2. Parameters and values used in the qualitative ecosystem model.

To isolate the effect of bacterial and viral proliferative genes on algal, coral, bacteria, and viral populations, as many parameters as possible were held constant, and only those relating directly to bacterial and viral proliferation and pathogenicity changed (listed in **bold**). All populations, shown with arbitrary units to show relative change in Figure 5, were initialized at 0.5. Note that, to account for finite space on the benthos, algal population size A is solved from coral population size C as A = 1 – C each iteration. Code can be found at *https://github.com/hopefulmonstersucla/viral-metabolism/tree/main/code*.

Level 2 Category	Photosystem	Function	Gene	Rho
Electron transport and photophosphorylation	Photosystem_II	photosystem II protein D1	PsbA	-0.845344
Electron transport and photophosphorylation	Photosystem_II	photosystem II protein D2	PsbD	-0.7327776
Electron transport and photophosphorylation	Photosystem_II	Cytochrome b559 beta chain	PsbF	-0.3442652
Electron transport and photophosphorylation	Photosystem_II	Photosystem II 10 kDa phosphoprotein	PsbH	0.04303315
Electron transport and photophosphorylation	Photosystem_II	Photosystem II protein	PsbN	-0.400914
Electron transport and photophosphorylation	Photosystem_II	Photosynthetic reaction center H subunit		-0.1290994
Electron transport and photophosphorylation	Photosystem_II	Putative photosynthetic complex assembly protein		0.2581989
Electron transport and photophosphorylation	Photosystem_I	photosystem I P700 chlorophyll a apoprotein subunit Ia	PsaA	-0.5610839
Electron transport and photophosphorylation	Photosystem_I	photosystem I P700 chlorophyll a apoprotein subunit Ib	PsaB	-0.6837071
Electron transport and photophosphorylation	Photosystem_I	photosystem I iron-sulfur center subunit VII	PsaC	-0.4461846
Electron transport and photophosphorylation	Photosystem_I	photosystem I subunit II	PsaD	-0.5711162
Electron transport and photophosphorylation	Photosystem_I	photosystem I subunit IV	PsaE	-0.502189
Electron transport and photophosphorylation	Photosystem_I	photosystem I subunit III plastocyanin docking protein	PsaF	-0.04303315
Electron transport and photophosphorylation	Photosystem_I	photosystem I subunit IX	PsaJ	-0.3442652
Electron transport and photophosphorylation	Photosystem_I	photosystem I subunit X	PsaK	-0.2484191
Light-harvesting complexes	Bacterial_light-harvesting_proteins	Light-harvesting LHI, beta subunit		0.1290994
Light-harvesting complexes	Chlorosome	Chlorosome protein I, 2Fe-2S ferredoxin		-0.2151657
Rhodopsins	Bacteriorhodopsin	Brp-like protein		-0.1844696
Rhodopsins	Proteorhodopsin	Octaprenyl-diphosphate synthase		0.1290994
Rhodopsins	Proteorhodopsin	Proteorhodopsin		-0.4655338

Supplementary Table 3. The frequency of photosynthesis genes across the lytic-temperate spectrum.

Genes were identified using SEED Level 2 categorization and are organized according to the KEGG photosynthesis map. Spearman's Rho values indicate whether genes are over-represented (value < 0) or under-represented (value > 0) in lytic versus temperate viral communities.

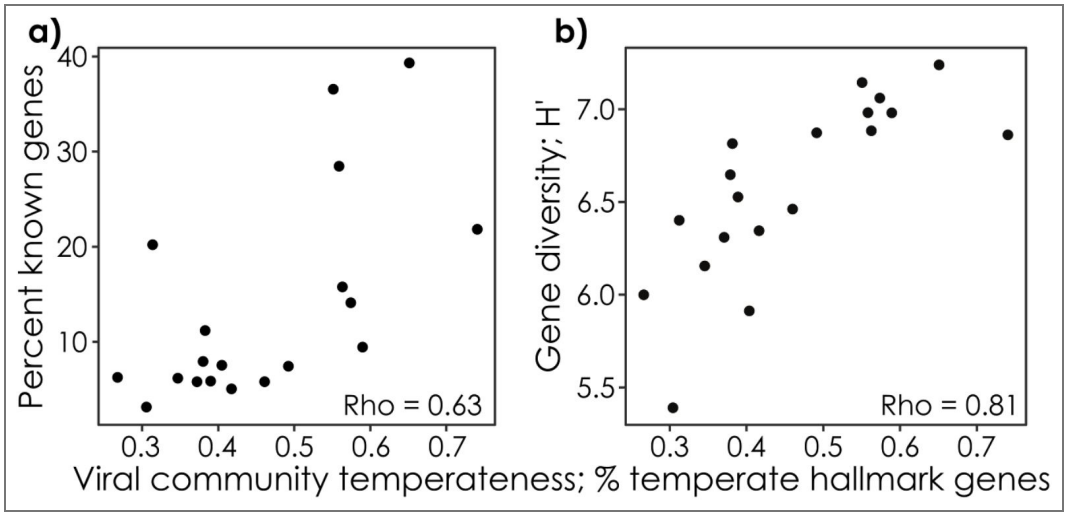

Supplementary Figure 1. Temperate viral communities are more cell-like and are more genetically diverse in known genes.

(a) The percent of genes with hits against the SEED database (i.e., percent known genes), and (b) the diversity of those known genes in the viral communities across the lytic to temperate spectrum. Note that the percent known genes is indicative of how metabolically similar the viruses are to cells given that known genes are commonly of identified in the study of cells. Viral community temperateness was calculated as the percentage of integrase and excision genes in the known genes in each virome.

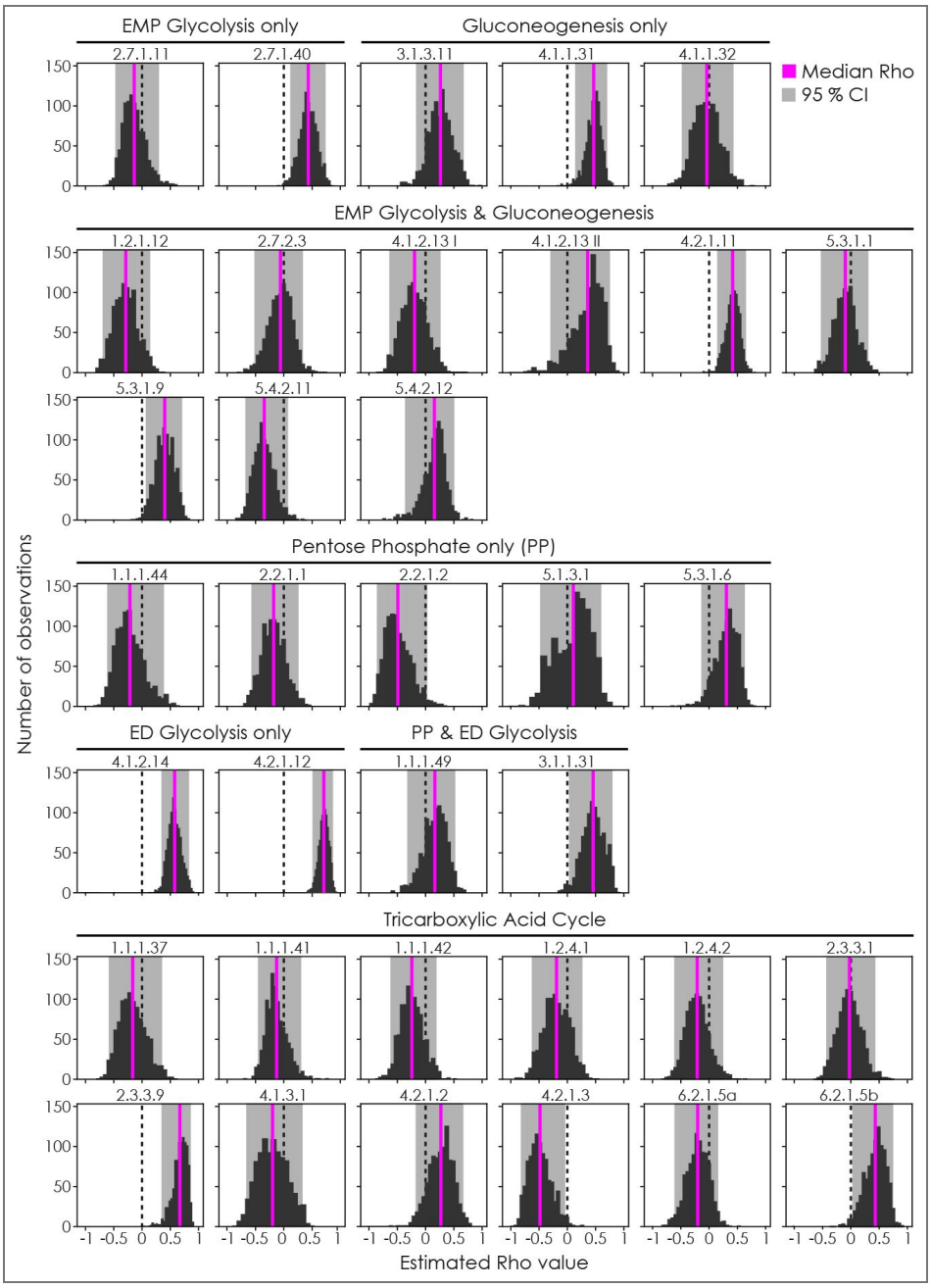

Supplementary Figure 2. Bootstrapped distribution of ρ_S from 1,000 iterations correlating the frequency of central carbon metabolism genes with viral community temperateness (number of observations vs ρ_S value).

Genes are grouped by pathway. Histogram shows the distribution of bootstrapped ρ_S values, with pink lines showing the median bootstrapped value and shaded grey areas showing the 95 % confidence interval of the median ρ_S. Dashed vertical lines show $\rho_S = 0$. Bootstrapping code can be found at *https://github.com/hopefulmonstersucla/viral-metabolism/tree/main/code*.

Acknowledgements

This work was supported by a BIG Summer stipend from Simons Foundation (awarded to Alexander Hoffmann for CU and NY) as well as by NSF Award OCE-2201645 to BK that provided Hopeful Monsters Summer stipends to JK, MK, GD, NF, EG, AK, and IT. LWK was supported by NSF award OCE-2118617. RAE was supported by an award from the NIH NIDDK RC2DK116713, an award from the Australian Research Council DP220102915, and an award from the Gordon and Betty Moore Foundation number 9871 (Perpetual Viral Origins). JG was supported by NSF Biology Integration Institute award 2119968. ML was supported by an NSF Postdoctoral Research Fellowship in Biology award 2209377. The authors would like to thank the captain, crew, and staff of the *NOAAS Hi'ialakai* (R 334) and National Oceanic and Atmospheric Administration (NOAA) shore support, as well as the members of the Pacific Reef Assessment and Monitoring Program of NOAA's National Coral Reef Monitoring Program.

Additional information

Funding

Funder	Grant reference number	Author
US National Science Foundation	2201645	Ben Knowles

Author ORCID iDs

Ben Knowles: https://orcid.org/0000-0002-0800-102X

References

1. **Haas AF,** et al. (2016) Global microbialization of coral reefs. *Nat Microbiol* **1**:1-7 https://doi.org/10.1038/nmicrobiol.2016.42 | PubMed
2. **McDole T,** et al. (2012) Assessing Coral Reefs on a Pacific-Wide Scale Using the Microbialization Score. *PLoS ONE* **7**:e43233 https://doi.org/10.1371/journal.pone.0043233 | PubMed
3. **Nelson CE,** Wegley Kelly L, Haas AF (2023) Microbial interactions with dissolved organic matter are central to coral reef ecosystem function and resilience. *Annu Rev Mar Sci* **15**:431-460 https://doi.org/10.1146/annurev-marine-042121-080917 | PubMed
4. **Haas AF,** et al. (2013) Influence of coral and algal exudates on microbially mediated reef metabolism. *PeerJ* **1**:e108 https://doi.org/10.7717/peerj.108 | PubMed
5. **McDole Somera T,** et al. (2016) Energetic differences between bacterioplankton trophic groups and coral reef resistance. *Proc R Soc B Biol Sci* **283**:20160467 https://doi.org/10.1098/rspb.2016.0467 | PubMed
6. **Smith JE,** et al. (2006) Indirect effects of algae on coral: algae-mediated, microbe-induced coral mortality. *Ecol Lett* **9**:835-845 https://doi.org/10.1111/j.1461-0248.2006.00937.x | PubMed
7. **Barott KL,** Rohwer FL (2012) Unseen players shape benthic competition on coral reefs. *Trends Microbiol* **20**:621-628 https://doi.org/10.1016/j.tim.2012.08.004 | PubMed
8. **Roach TN,** et al. (2017) Microbial bioenergetics of coral-algal interactions. *PeerJ* **5**:e3423 https://doi.org/10.7717/peerj.3423 | PubMed
9. **Nelson CE,** et al. (2013) Coral and macroalgal exudates vary in neutral sugar composition and differentially enrich reef bacterioplankton lineages. *ISME J* **7**:962-979 https://doi.org/10.1038/ismej.2012.161 | PubMed
10. **Silveira CB,** et al. (2017) Microbial processes driving coral reef organic carbon flow. *FEMS Microbiol Rev* **41**:575-595 https://doi.org/10.1093/femsre/fux018 | PubMed

11. **Flamholz A,** Noor E, Bar-Even A, Liebermeister W, Milo R (2013) Glycolytic strategy as a tradeoff between energy yield and protein cost. *Proc Natl Acad Sci* **110**:10039-10044 https://doi.org/10.1073/pnas.1215283110 | PubMed
12. **Thingstad TF** (2000) Elements of a theory for the mechanisms controlling abundance, diversity, and biogeochemical role of lytic bacterial viruses in aquatic systems. *Limnol Oceanogr* **45**:1320-1328 https://doi.org/10.4319/lo.2000.45.6.1320
13. **Knowles B,** et al. (2016) Lytic to temperate switching of viral communities. *Nature* **531**:466-470 https://doi.org/10.1038/nature17193 | PubMed
14. **Suttle C** (2007) a. Marine viruses--major players in the global ecosystem. *Nat Rev Microbiol* **5**:801-12 https://doi.org/10.1038/nrmicro1750 | PubMed
15. **Fuhrman J** (1999) a. Marine viruses and their biogeochemical and ecological effects. *Nature* **399**:541-8 https://doi.org/10.1038/21119 | PubMed
16. **Silveira CB,** et al. (2023) Viral predation pressure on coral reefs. *BMC Biol* **21**:77 https://doi.org/10.1186/s12915-023-01571-9 | PubMed
17. **Friman V.-P,** Buckling A (2014) Phages can constrain protist predation-driven attenuation of Pseudomonas aeruginosa virulence in multienemy communities. *ISME J* **8**:1820-1830 https://doi.org/10.1038/ismej.2014.40 | PubMed
18. **Aijaz I,** Koudelka GB (2019) Cheating, facilitation and cooperation regulate the effectiveness of phage-encoded exotoxins as antipredator molecules. *Microbiologyopen* **8**:e00636 https://doi.org/10.1002/mbo3.636 | PubMed
19. **Brüssow H** (2007) Bacteria between protists and phages: from antipredation strategies to the evolution of pathogenicity. *Mol Microbiol* **65**:583-589 https://doi.org/10.1111/j.1365-2958.2007.05826.x | PubMed
20. **Cram J,** Parada A, Fuhrman J (2016) Dilution reveals how viral lysis and grazing shape microbial communities. *Limnol Oceanogr* **61**:889-905 https://doi.org/10.1002/lno.10259
21. **Fuhrman JA,** Noble RT (1995) Viruses and protists cause similar bacterial mortality in coastal seawater. *Limnol Oceanogr* **40**:1236-1242 https://doi.org/10.4319/lo.1995.40.7.1236
22. **Knowles B,** Rohwer F (2017) Knowles & Rohwer Reply. *Nature* **549**:E3-E4 https://doi.org/10.1038/nature23296 | PubMed
23. **Breitbart M,** Bonnain C, Malki K, Sawaya NA (2018) Phage puppet masters of the marine microbial realm. *Nat Microbiol* **3**:754-766 https://doi.org/10.1038/s41564-018-0166-y | PubMed
24. **Brum JR,** et al. (2015) Patterns and ecological drivers of ocean viral communities. *Science* **348**:1261498 https://doi.org/10.1126/science.1261498 | PubMed
25. **Hurwitz BL,** U'Ren JM (2016) Viral metabolic reprogramming in marine ecosystems. *Curr Opin Microbiol* **31**:161-168 https://doi.org/10.1016/j.mib.2016.04.002 | PubMed
26. **Howard-Varona C,** et al. (2020) Phage-specific metabolic reprogramming of virocells. *ISME J* **14**:881-895 https://doi.org/10.1038/s41396-019-0580-z | PubMed
27. **Roach TN,** et al. (2020) A multiomic analysis of in situ coral–turf algal interactions. *Proc Natl Acad Sci* **117**:13588-13595 https://doi.org/10.1073/pnas.1915455117 | PubMed
28. **Thompson LR,** et al. (2011) Phage auxiliary metabolic genes and the redirection of cyanobacterial host carbon metabolism. *Proc Natl Acad Sci U S A* **108**:E757-64 https://doi.org/10.1073/pnas.1102164108 | PubMed
29. **Thompson LR,** Zeng Q, Chisholm SW (2016) Gene expression patterns during light and dark infection of Prochlorococcus by cyanophage. *PloS One* **11**:e0165375 https://doi.org/10.1371/journal.pone.0165375 | PubMed
30. **Roitman S,** et al. (2015) Closing the gaps on the viral photosystem-I psa DCAB gene organization. *Environ Microbiol* **17**:5100-5108 https://doi.org/10.1111/1462-2920.13036 | PubMed

31. **Lehninger AL** (1965) Bioenergetics. The molecular basis of biological energy transformations. https://www.cabidigitallibrary.org/doi/full/10.5555/19671403907
32. **Baer J,** et al. (2025) Viralization as a microbial approach for enhancing coral reef restoration. *ISME J* **19**:wraf110 https://doi.org/10.1093/ismejo/wraf110 | PubMed
33. **Haas AF,** et al. (2014) Unraveling the unseen players in the ocean-a field guide to water chemistry and marine microbiology. *JoVE J Vis Exp* e52131 https://doi.org/10.3791/52131 | PubMed
34. **Sambrook J,** Fritsch EF, Maniatis T (1989) *Molecular Cloning: A Laboratory Manual* Cold Spring Harbor Laboratory Press.
35. **Thurber RV,** Haynes M, Breitbart M, Wegley L, Rohwer F (2009) Laboratory procedures to generate viral metagenomes. *Nat Protoc* **4**:470-483 https://doi.org/10.1038/nprot.2009.10 | PubMed
36. **Lücking D,** Mercier C, Alarcón-Schumacher T, Erdmann S (2023) Extracellular vesicles are the main contributor to the non-viral protected extracellular sequence space. *ISME Commun* **3**:112 https://doi.org/10.1038/s43705-023-00317-6 | PubMed
37. **Schmieder R,** Edwards R (2011) Quality control and preprocessing of metagenomic datasets. *Bioinformatics* **27**:863-864 https://doi.org/10.1093/bioinformatics/btr026 | PubMed
38. **Schmieder R,** Lim YW, Rohwer F, Edwards R (2010) TagCleaner: Identification and removal of tag sequences from genomic and metagenomic datasets. *BMC Bioinformatics* **11**:1-14 https://doi.org/10.1186/1471-2105-11-341 | PubMed
39. **Schmieder R,** Edwards R (2011) Fast identification and removal of sequence contamination from genomic and metagenomic datasets. *PloS One* **6**:e17288 https://doi.org/10.1371/journal.pone.0017288 | PubMed
40. **Meyer F,** et al. (2008) The metagenomics RAST server – a public resource for the automatic phylogenetic and functional analysis of metagenomes. *BMC Bioinformatics* **9**:386 https://doi.org/10.1186/1471-2105-9-386 | PubMed
41. **Kelly LW,** et al. (2011) Black reefs: iron-induced phase shifts on coral reefs. *ISME J* **6**:1-12 https://doi.org/10.1038/ismej.2011.114 | PubMed
42. **Barott KL,** et al. (2012) Microbial to reef scale interactions between the reef-building coral Montastraea annularis and benthic algae. *Proc R Soc B Biol Sci* **279**:1655-1664 https://doi.org/10.1098/rspb.2011.2155 | PubMed
43. **George EE,** et al. (2021) Space-filling and benthic competition on coral reefs. *PeerJ* **9**:e11213 https://doi.org/10.7717/peerj.11213 | PubMed
44. **Barott K,** et al. (2009) Hyperspectral and physiological analyses of coral-algal interactions. *PloS One* **4**:e8043 https://doi.org/10.1371/journal.pone.0008043 | PubMed
45. **Pirovich DB,** Da'dara AA, Skelly PJ (2021) Multifunctional fructose 1, 6-bisphosphate aldolase as a therapeutic target. *Front Mol Biosci* **8**:719678 https://doi.org/10.3389/fmolb.2021.719678 | PubMed
46. **Webb EC** (1992) *Enzyme Nomenclature 1992 Recommendations of the Nomenclature Committee of the International Union of Biochemistry and Molecular Biology on the Nomenclature and Classification of Enzymes* Academic Press.
47. **Srinivasan P,** Katagiri M, Sprinson DB (1959) The conversion of phosphoenolpyruvic acid and d-erythrose 4-phosphate to 5-dehydroquinic acid. *J Biol Chem* **234**:713-715 https://doi.org/10.1016/s0021-9258(18)70160-9 | PubMed
48. **Knowles B,** et al. (2017) Variability and host density independence in inductions-based estimates of environmental lysogeny. *Nat Microbiol* **2**:17064 https://doi.org/10.1038/nmicrobiol.2017.64 | PubMed
49. **Knowles B,** et al. (2020) Temperate infection in a virus–host system previously known for virulent dynamics. *Nat Commun* **11**:1-13 https://doi.org/10.1038/s41467-020-18078-4 | PubMed

50. **Howard-Varona C,** Hargreaves KR, Abedon ST, Sullivan MB (2017) Lysogeny in nature: mechanisms, impact and ecology of temperate phages. *ISME J* **11**:1511 https://doi.org/10.1038/ismej.2017.16 | PubMed

51. **Hurwitz BL,** Hallam SJ, Sullivan MB (2013) Metabolic reprogramming by viruses in the sunlit and dark ocean. *Genome Biol* **14**:1-14 https://doi.org/10.1186/gb-2013-14-11-r123 | PubMed

52. **Michniewski SE,** et al. (2021) A new family of "megaphages" abundant in the marine environment. *Nat Microbiol* **1**:58 https://doi.org/10.1038/s43705-021-00064-6 | PubMed

53. **Anantharaman K,** et al. (2014) Sulfur oxidation genes in diverse deep-sea viruses. *Science* **344**:757-760 https://doi.org/10.1126/science.1252229 | PubMed

54. **Moniruzzaman M,** Martinez-Gutierrez CA, Weinheimer AR, Aylward FO (2020) Dynamic genome evolution and complex virocell metabolism of globally-distributed giant viruses. *Nat Commun* **11**:1710 https://doi.org/10.1038/s41467-020-15507-2 | PubMed

55. **Ha AD,** Moniruzzaman M, Aylward FO (2021) High transcriptional activity and diverse functional repertoires of hundreds of giant viruses in a coastal marine system. *mSystems* **6**:e0074321 https://doi.org/10.1128/msystems.00293-21 | PubMed

56. **Rodrigues RAL,** Arantes TS, Oliveira GP, Silva LK, Abrahão JS (2019) The complex nature of Tupanviruses. *Adv Virus Res* **103**:135-162 https://doi.org/10.1016/bs.aivir.2018.09.001 | PubMed

57. **Bachy C,** others (2021) Viruses infecting a warm water picoeukaryote shed light on spatial and temporal patterns in virus community ecology. *ISME J* **15**:3129-3137 https://doi.org/10.1038/s41396-021-00989-9 | PubMed

Peer reviews

Reviewer #1 (Public review):

Summary:

Microbialization (bacterial overgrowth) is a recognized component of degraded, eutrophied coral reefs where there is a shift from coral to algal dominance on the benthos. In addition, previous work has demonstrated that virus communities shift from a lytic strategy dominated (kill-the-winner) to a temperate (lysogenic) strategy dominated with reef microbialization. Kelman et al. sought to leverage previously published virus metagenomes produced from the water column of healthy and degraded coral reefs to assess virus community metabolic shifts. The authors also produce a conceptual model to demonstrate the potential impact of the observed metabolism shifts on reef fates.

Strengths:

The main strength of the manuscript is the findings from their metagenomic analyses and results. The virus metagenomes were produced using established approaches in the field and yield sufficient data per sample for their analyses. Interesting results regarding the shift in the types of genes from anaplerotic to cataplerotic provide the foundation for testable hypotheses to determine the magnitude of impact virus strategies have on reef health. The introduction is also well written and sets up the scene very well.

Weaknesses:

(1) The methods text currently omits important information related to the sampling design. It is not clear how many metagenomes are from healthy and degraded communities. This impacts the interpretability and robustness of the statistical results. Furthermore, it is unclear if analyses are based on assembled contigs or read-based alignments. Improving the clarity and organization of the Methods is essential for reproducibility.

(2) Regarding the bioinformatics approach, normalization using the "percent known" approach within samples may not fully account for discovery bias related to sequencing depth. While Supplementary Table 1 shows variability in read counts, the lack of community-level metadata makes it difficult to determine if sequencing depth covaries with community type (healthy vs. degraded). The study would benefit from a rarefaction analysis or subsampling to ensure that gene frequency trends and Spearman correlations are biological signals rather than artifacts of sequencing effort.

(3) The qualitative model in Figure 5 is positioned as evidence for the role of viruses in reef health, but it does not provide independent support for the authors' hypotheses. Since the model is parameterized using "arbitrary units" to reflect the authors' assumptions rather than being derived from the empirical metagenomic data, it serves as a helpful illustration of a hypothesis but not as a validation of the findings.

(4) Results and discussion require revisions to improve readability and connectivity across sections. Ensuring a clear distinction between empirical data and model-based speculation would help the audience better appreciate the science.

https://doi.org/10.7554/eLife.110377.1.sa1

Reviewer #2 (Public review):

Summary:

The manuscript by Kelman and coauthors investigates how viral communities differ in the genes they encode in healthy and degraded coral reef ecosystems. Across 19 viral metagenomes from Central Pacific reefs, the authors assess the frequency of integration/excision genes as a proxy for viral community temperateness and ask whether genes associated with central carbon metabolism covary with signatures of temperateness. The main finding is that viral communities with more temperate-related genes encode more genes from the Entner-Doudoroff pathway and other reactions interpreted as anaplerotic, whereas more lytic-associated viral communities show greater representation of some pentose phosphate pathway, TCA, and redox-associated genes interpreted as cataplerotic. The authors propose a model based on these patterns in which lytic viral metabolism helps suppress bacterial overgrowth on healthy reefs, while temperate viral metabolism may promote microbialization on degraded reefs. The study addresses an interesting and potentially important concept - that viral auxiliary metabolic genes are important components of microbial communities and can affect ecosystem functioning. Linking viral metabolism to coral reef microbialization is a creative conceptual advance. The manuscript is clearly written, and the reported enrichment of anaplerotic genes in temperate-associated viromes is an interesting pattern that could motivate future work on how viral metabolic potential varies across reef states.

Strengths:

(1) The study connects viral lifestyle, central carbon metabolism, bacterial overgrowth, and reef degradation in a framework that could be useful for future studies of coral reef ecosystems and viral ecology. This is an interesting synthesis that links viral auxiliary metabolism to broader questions about microbialization and reef state.

(2) The manuscript is generally clearly organized around a testable prediction: viral metabolic gene content should vary along a lytic-to-temperate viral community gradient. The reported enrichment of anaplerotic genes in viromes with a larger fraction of temperate viruses is a compelling result.

(3) The authors highlight several virus-encoded metabolic genes that may not have been previously reported in viral datasets or genomes. If supported by further validation, these observations could expand the known repertoire of viral metabolic potential.

(4) The modeling helps clarify the feedbacks the authors propose may connect viral lifestyle, bacterial metabolism, and coral reef degradation. It provides a foundation for generating hypotheses about how viral metabolic genes could influence reef microbial dynamics.

Weaknesses:

(1) The main limitation is that the evidence for several key claims remains indirect. The core analysis is based on correlations between metabolic gene frequencies and integration/excision-related genes. This does not demonstrate that the metabolic genes occur in temperate viral genomes, are physically linked to lysogeny genes, are expressed during infection, or alter host metabolism. Thus, the data support an association between VLP-associated metabolic annotations and a community-level temperateness proxy, but not a direct link between temperate phages and these metabolic functions.

(2) It is important not to equate community-level gene frequencies with genome-level or infection-level metabolic programs. A virome may contain more anaplerotic genes overall, but that does not demonstrate that individual viruses reprogram their hosts in an anaplerotic manner nor that infection produces a net anaplerotic effect. Individual viruses may encode both anaplerotic and cataplerotic genes, and a smaller number of cataplerotic genes could have stronger metabolic consequences depending on expression, enzyme efficiency, pathway position, and host context. This is an important limitation that should be acknowledged and, if possible, addressed with contig- or genome-level analyses.

(3) The ecological interpretation assumes that viral infection is strong enough to influence reef-scale bacterial population dynamics. However, the study does not directly measure infection frequency, lysis rates, viral production, burst size, lysogeny frequency, prophage induction, gene expression, or bacterial mortality. If viral mortality or lysogenic conversion were rare in these systems, the observed gene-frequency patterns could have limited ecosystem-level consequences. This makes claims about viral metabolism suppressing bacterial overgrowth, accelerating microbialization, or acting as a conservation lever more speculative than suggested.

(4) There are statistical limitations related to the use of relative gene frequencies. Because genes are normalized as percentages of known genes, the data are compositional. Apparent increases in some categories may partly reflect decreases in others. Bootstrapped Spearman correlations are useful for assessing the robustness of these associations, but they do not address compositionality or multiple testing.

(5) The anaplerotic/cataplerotic classification is central to the manuscript's conclusions and would benefit from more support. The framework is useful, but it depends on both annotation confidence and biochemical context. Sequence-similarity annotations alone may be vulnerable to misannotation, especially for central metabolic enzymes that share conserved domains across functionally distinct proteins. Stronger evidence that key genes contain key functional domains and/or are phylogenetically related to characterized enzymes would help support the proposed functions. In addition, many central carbon enzymes are reversible or context-dependent, so a clearer rationale for each classification would strengthen the interpretation.

Overall, the manuscript presents a valuable hypothesis and highlights new ecological patterns in coral reef viral metagenomes, but falls short of the evidence needed for the strongest claims. The work would be strengthened by analyses that directly link metabolic genes to viral genomes or lysogeny markers, address compositional effects, validate key

annotations, and more clearly distinguish observed gene-frequency associations from hypothesized effects on infection, host metabolism, and reef state.

https://doi.org/10.7554/eLife.110377.1.sa0